Journal of
Materials Chemistry A

Accepted Manuscript

This is an *Accepted Manuscript*, which has been through the RSC Publishing peer review process and has been accepted for publication.

Accepted Manuscripts are published online shortly after acceptance, which is prior to technical editing, formatting and proof reading. This free service from RSC Publishing allows authors to make their results available to the community, in citable form, before publication of the edited article. This *Accepted Manuscript* will be replaced by the edited and formatted *Advance Article* as soon as this is available.

To cite this manuscript please use its permanent Digital Object Identifier (DOI®), which is identical for all formats of publication.

More information about *Accepted Manuscripts* can be found in the **Information for Authors**.

Please note that technical editing may introduce minor changes to the text and/or graphics contained in the manuscript submitted by the author(s) which may alter content, and that the standard **Terms & Conditions** and the **ethical guidelines** that apply to the journal are still applicable. In no event shall the RSC be held responsible for any errors or omissions in these *Accepted Manuscript* manuscripts or any consequences arising from the use of any information contained in them.

Towards balanced strength and toughness improvement of isotactic polypropylene nanocomposites by surface functionalized graphene oxide

Rui-Ying Bao, Jun Cao, Zheng-Ying Liu, Wei Yang, Bang-Hu Xie, Ming-Bo Yang*

College of Polymer Science and Engineering, Sichuan University, State Key Laboratory of Polymer Materials Engineering, Chengdu, 610065, Sichuan, China

Abstract

Balanced stiffness and toughness is always the goal of high-performance general plastics for engineering purposes and the interfacial crystalline structure control has been proved to be an effective way to approach this goal. In this work, a kind of novel β-nucleating agent (β-NA) for isotactic polypropylene (iPP), one of the most rapidly developing general plastics, was supported onto the surface of octadecylamine functionalized graphene oxide (GO-D), and the effects of functionalized graphene oxide (GO) on the crystallization behavior, crystalline structures and mechanical properties of iPP composites were studied. The presence of the octadecyl chain changes the hydrophilic GO to be hydrophobic, and further supporting of β-NA on GO-D (GO-N) does not change its solubility in xylene. The hydrophobic nature of octadecyl chains on the GO-D and GO-N surface leads to improved interfacial adhesion with the non-polar iPP matrix. At the same time, GO-N exhibit high efficiency in inducing the formation of β crystals of iPP. The relative content of β crystals, k_β, reaches a value as high as 73.6% at a loading of 0.1 wt% GO-N, resulting in a maximum increase in impact strength by almost 100% and a simultaneous improvement of the tensile strength

* Corresponding author. Tel.: + 86 28 8546 0130; fax: + 86 28 8546 0130.

E-mail address: weiyang@scu.edu.cn (W Yang)

by about 30%. This work provides a potential industrializable technique for high-performance iPP nanocomposites.

Introduction

Isotactic polypropylene (iPP), a typical polymorphic thermoplastic with several crystalline forms including monoclinic (α), trigonal (β) and orthorhombic (γ) [1, 2], is one of the most important and rapidly developing thermoplastic polymers due to its low cost and versatility [3, 4]. The β form iPP (β-iPP) shows excellent toughness and thermal performance [2], and has received much attention in scientific researches and industrial applications. However, β-iPP can only be formed under some special conditions such as quenching the melt to a certain temperature range [5], directional crystallization in a temperature gradient field [6], melt shear or elongation [7], or with the help of selective β-nucleating agent (β-NA) [8, 9]. Among these methods, the addition of β-NA is the simplest and the most effective to obtain a high content of β crystals. Although β-iPP shows superior toughness and thermal performance, its yield strength and stiffness are generally much lower than those of α form iPP (α-iPP) [1, 2, 10]. To improve the stiffness of β-iPP, the combined modification of iPP with reinforcing fillers and β-NA may be a possible path to balance the stiffness-toughness of iPP [11, 16].

Graphene, as an atomically thick, two-dimensional sheet composed of sp^2 carbon atoms arranged in a honeycomb structure, has attracted a tremendous amount of attention due to its fascinating properties such as super mechanical, electrical and thermal properties[11-15]. It has been widely studied in various fields including energy devices [16-18], sensors [19, 20], catalysts [21, 22], electronic materials [23], drug delivery [24] and polymer composites[25-28]. Compared with other nanofillers for

reinforcing purpose in polymer composites, graphene is considered to be an optimum choice for its abundant source of raw material as well as superior properties.

As a precursor of graphene, graphene oxide (GO) is easily available through the controlled chemical oxidation of graphite and can be easily reduced to graphene by chemical or thermal approaches[29, 30]. It is believed that GO should be more preferred in reinforcing polymers than graphene because the functional groups on the surface of GO sheets can enhance the compatibility between GO and polymer matrix. GO contains graphitic domains and oxidation regions, with epoxide and hydroxyl groups locating on the basal planes and carbonyl and carboxyl groups at the edges [31, 32]. The presence of these functional groups endows GO with strong hydrophilicity and allows for enhanced interactions with polar polymers such as poly (methyl methacrylate) [33], polyamide[27] and poly(vinyl alcohol) [34]. However, GO requires surface modification to be homogenously dispersed in non-polar polymers. Surface modification of GO can be realized easily by the introduction of functional groups such as epoxide and carboxyl groups [35, 36]. The functionalized GO showed good dispersion in non-polar polymers, such as polystyrene [37] and iPP [38]. The formation of a polymer crystalline layer surrounding nanofillers is another route to enhance a non-covalent interface between nanofillers and a semi-crystalline polymer for stress transfer,[39, 40] and GO shows α-nucleating ability for the crystallization of iPP. [41, 42]

In this work, a kind of novel β-NA for iPP synthesized by our group [43], N,N′-Dicyclohexyl-1,5-diamino-2,6-naphthalenedicarboxamide, was supported onto the surface of octadecylamine functionalized GO (GO-D), aiming at balanced reinforcing and toughening of iPP. The effects of functionalized GO on the crystallization behavior, crystalline structures and mechanic

properties of iPP nanocomposites were studied. The interfacial adhesion between GO and non-polar iPP matrix was found to be improved by surface functionalization, and the β-NA functionalized GO showed high efficiency in inducing the formation of β crystals, exhibiting huge influence on the mechanical properties of iPP nanocomposites.

Experimental Section

Materials

iPP with a trade name of T30S and a melt flow rate of 2.3 g/10min (230 °C, 2.16 kg load) was purchased from Lanzhou petroleum Chemical Co, Ltd. (PR China). β-NA was synthesized according to the procedure reported in our previous work[43]. Natural flake graphite (NG) with an average particle size of 200 meshes and a purity of over 99.9% was purchased from Shenghua Research Institute (Changsha, China). Sodium nitrate ($NaNO_3$), potassium permanganate ($KMnO_4$), concentrated sulfuric acid (H_2SO_4), hydrochloric acid (HCl), hydrazine hydrate (80%), hydrogen peroxide (H_2O_2), ODA, ethanol and xylene were purchased from Chengdu Changzheng Chemical Glass Apparatus Co, Ltd. (PR China) and used as received.

Surface functionalization of GO

Graphite oxide was synthesized from NG powder by modified Hummer's method.[44, 45] Graphite oxide was exfoliated into GO under ultrasonication according to the method in our previous work.[46] Briefly, the obtained graphite oxide powder (0.5g) was added to a given amount of deionized water (500 ml), and then the mixture was subjected to bath ultrasonication (KQ-400KDB, 40 kHz, 400 W) and mechanical stirring for 1 h. Subsequently, the resulting homogeneous dispersion was freeze-dried in a lyophilizer to remove all the water. The resulting powdery samples were named as

GO.

For the grafting of ODA on GO, the resulting suspension under ultrasonication in the last step was mixed with the solution of ODA (0.9g) in 90 ml of ethanol. [37, 47, 48] The mixture was refluxed under stirring for 20 h at 90 °C and vacuum filtrated. The obtained powder was re-dispersed in 100 ml of warm ethanol under ultrasonication for 5 min and vacuum filtrated. The rinsing-filtration cycle was repeated for four times to remove excess and physically adsorbed ODA. At last, resulted ODA grafted GO powder (designated as GO-D) was vacuum dried at 60 °C for 24 h.

For the supporting of β-NA onto GO-D, 50 mg of GO-D powder was dispersed in 100 ml of xylene under magnetic stirring. Then GO-D dispersion was mixed with xylene solution of 50 mg β-NA and stirred overnight. Obtained from the mixture by vacuum filtration, the solids were re-dispersed in 200 ml of xylene and separated by vacuum filtration again. This purification cycle was repeated for four times to ensure that the filtrate is free of dissociative β-NA, and the final products were dried at 40 °C under vacuum overnight, yielding GO-D supported β-NA (designated as GO-N), a functionalized GO with β-NA on the surface.

Preparation of iPP composites

Various iPP composites were prepared by solution mixing. In brief, the desired amount of GO-N (0.1, 0.2, 0.5 wt%, respectively) was dispersed in xylene homogeneously by ultrasonication at room temperature for 30 min. In a three neck round flask, the desired amount of iPP was dissolved in xylene at 130 °C to obtain a solution. The dispersion of GO-N was then dropped into the iPP solution and stirred for 30 min. Finally, the composite solution was dropped into vigorous stirring methanol to coagulate the iPP composites. The precipitate was obtained by filtrating and drying in a vacuum oven

at 70 °C for 3 days. For comparison, pure iPP, iPP composites with 0.1 wt% GO and 0.1 wt% GO-D were also prepared with the same procedure. These samples were compression molded at 200 °C and 10 MPa into rectangular specimens (80 mm length ×10 mm width × 4 mm thickness) for impact testing or sheets (80 mm length ×10 mm width × 0.5 mm thickness). The specimens for tensile tests were then prepared by cutting these sheets into dog-bone type samples (7 mm width × 15 mm gauge length × 0.5 mm thickness).

Characterization

The chemical characteristics of GO, GO-D and GO-N were analyzed by X-ray photoelectron spectrometer (XPS) (XSAM800, Kratos Company, UK) using Mg Kα as the radiation source (hv=1253.6 eV).

Non-isothermal crystallization behaviors of the composites were studied by differential scanning calorimeter (DSC) with a DSC Q20 (TA Instruments, USA) under a nitrogen gas flow of 50 mL min^{-1}. Samples of about 3-5 mg were melted at 200 °C for 5 min; then the melt was cooled down to 40 °C to record the crystallization behavior, and heated again to 200 °C to record the melting behavior. The cooling and heating rates were 10 °C/min.

X-ray diffraction (XRD) profiles were recorded on a DX-1000 X-ray diffractometer (Dandong Fanyuan Instrument Co. LTD) using a CuKα radiation source (λ= 0.154 nm, 40 kV, 25 mA) in the scanning angle range of 2θ=2-45° at a scan speed of 3 °/min. The relative content of β crystals (k_β) in the crystalline phase was evaluated according to Turner-Jones et al.[5]

$$k_\beta = H_{\beta(300)}/(H_{\beta(300)}+H_{\alpha(110)}+H_{\alpha(040)}+H_{\alpha(130)})$$

where $H_{\alpha(110)}$, $H_{\alpha(040)}$ and $H_{\alpha(130)}$ are the intensities of the (110), (040) and (130) diffraction peaks of α

phase and correspond to 2θ=14.1, 16.9 and 18.6°, respectively, and $H_{\beta(300)}$ is the intensity of the (300) diffraction peak of β phase at 2θ=16.1°.

The morphology and thickness of GO, GO-D and GO-N were determined by AFM using a Nanoscope Multimode and Explore atomic force microscopy (Veeco Instruments, USA), in the tapping mode using rectangular cantilevers with a spring constant of ~ 40 N m^{-1} and the typical resonance frequencies between 250 and 300 kHz. A Tecnai G2 F20S-TWIN transmission electron microscope (TEM) was used to characterize the morphology of the filler dispersed in iPP matrix with an accelerating voltage of 200 kV. The supermolecular structures of pure iPP and iPP composites were observed using an XFORD 6650 scanning electron microscope (SEM) at an accelerating voltage of 20 kV. Before SEM characterization, the sample was etched for 12 h with an etchant containing 1.3 wt % potassium permanganate ($KMnO_4$), 32.9 wt % concentrated sulfuric acid (H_2SO_4), and 65.8 wt % concentrated phosphoric acid (H_3PO_4), according to the method developed by Olley et al[49]. All the samples were gold sputtered prior to SEM characterization.

Tensile tests were conducted on the dog-bone type specimens with an AGS-J universal testing machine (Shimadzu Instruments, Japan) according to ASTM d638-82a, and the crosshead speed was 50 mm/min. Notched impact strength was evaluated on a UJ-40 Izod impact test instrument (Chengde Jinjian Testing Instrument Co. Ltd., Heibei, China) according to ASTM D256 on the rectangular specimens. Further, the double-notch four-point-bend (DN-4-PB) technique was used to investigate the deformation history of the materials in the vicinity of the crack tip. The rectangular specimens were given two sharp identical notches using a razor blade. The distance between the two sharp notches on the DN-4-PB bar was set at 10 mm. The DN-4PB tests were performed to generate

subcritical fracture using the AGS-J universal testing machine at a crosshead speed of 10mm/min. The damage zone of the unbroken notch tip in the DN-4-PB test was observed using transmission optical microscope (TOM) (BX51, Olympus, Japan) after obtaining thin sections (20 μm). At least five samples were tested in all the tests conducted.

3 Results and Discussion

Surface functionalization of GO with β-NA

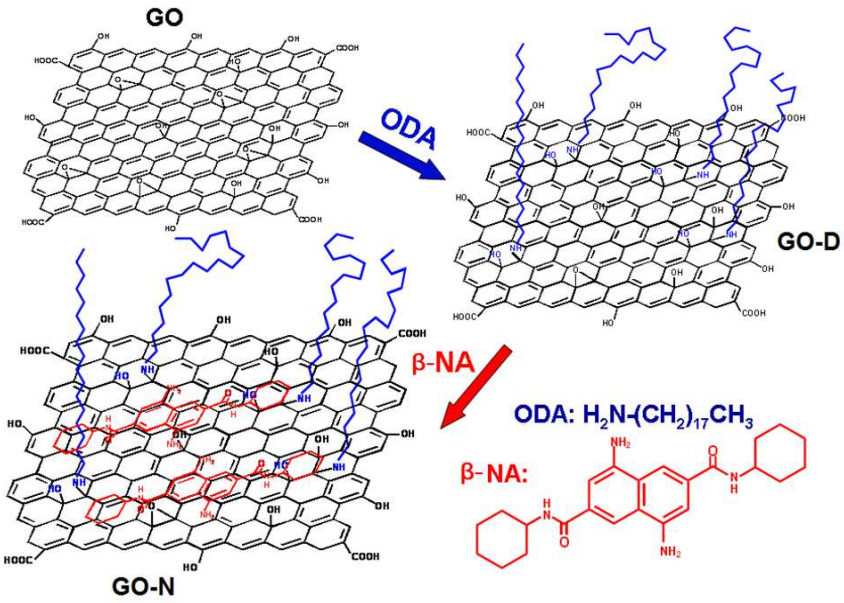

Fig. 1 Schematic for the proposed mechanism of functionalization of GO with β-NA.

The mechanism of functionalization of GO with β-NA is shown in Fig. 1. The hydrophilic groups on GO surface were converted to alkyl groups to disperse GO in organic solvent, and β-NA was then supported onto their basal plane through O-H···O or N-H···O hydrogen bonding. XPS was employed to evaluate the chemical change of GO surface brought by the functionalization and favorable interaction. The Lorentzian function is generally fitted to determine the peak shape after Shirley background correction. Fig. 2 shows the full XPS spectra and XPS spectra of GO, GO-D and

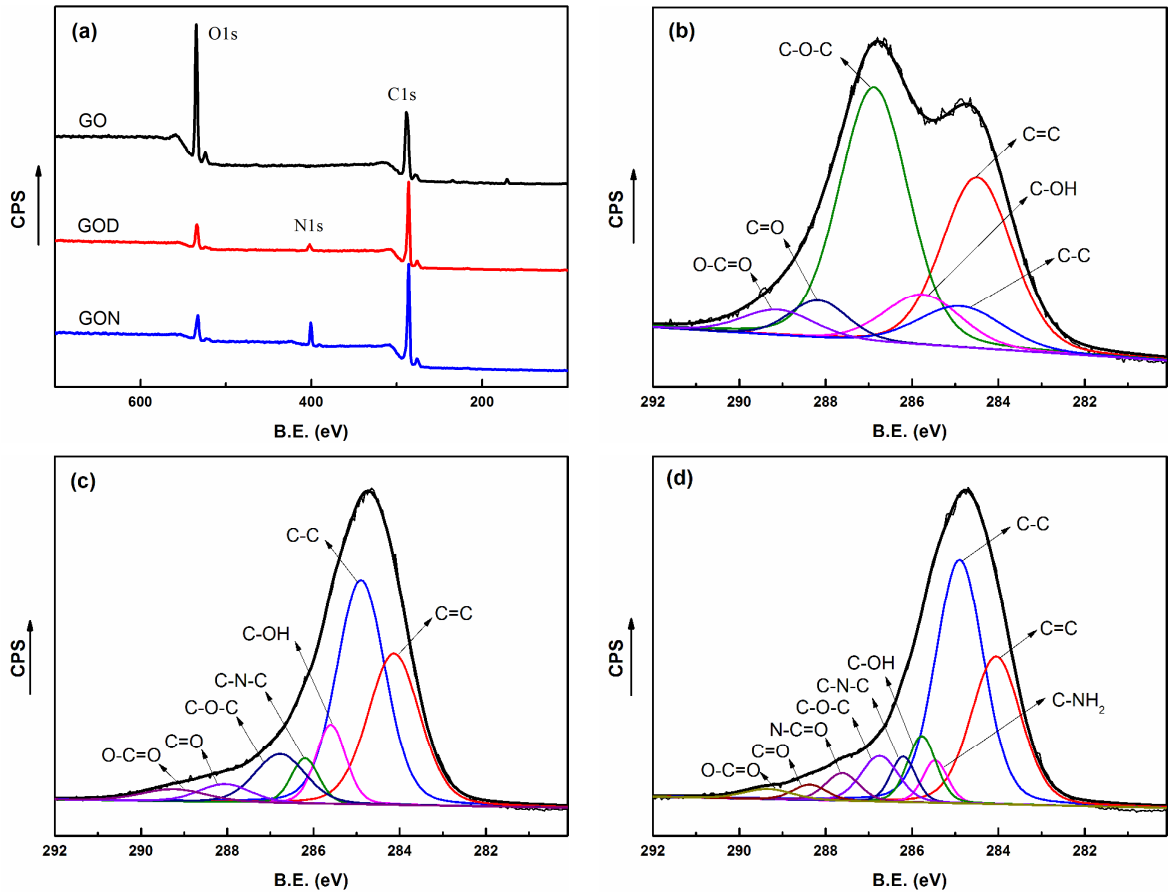

Fig. 2 XPS spectra: (a) full spectra of GO, GO-D and GO-N, and C1s of (b) GO, (c) GO-D and (d) GO-N

GO-N in the C1s region. The deconvoluted C1s peaks, with their relative atomic percentages, are shown in Table 1. The C1s XPS spectrum of GO (Fig.2b) consists of six different chemically shifted components and can be deconvoluted into: sp^2 C=C, sp^3 C-C in aromatic rings (284.5 and 284.9 eV); C-OH (285.8 eV); C-O-C (286.8 eV); C=O (288.2 eV); O-C=O (289.1 eV), respectively. These assignments agree with previous works.[50-52] In contrast, in the spectra of GO-D and GO-N (Fig.2c and d), the peak intensities corresponding to C-C increase significantly, while the peak intensities related to the oxidized carbon species reduced markedly. Furthermore, in Fig.2c, the emergence of new peaks corresponding to C-N-C (at 286.1 eV, Δ% is 4.68%)[52] is accompanied by a significant

decrease in those of C–O–C (at 286.8 eV, Δ% = -33.41%), demonstrating the reaction of GO with ODA through the nucleophilic substitution reaction between the amine group of ODA and the epoxide group of GO.[48] In Fig.2d, the new peaks at 285.4 eV and 287.4 eV assigning to C-NH_2 and N-C=O species of β-NA, respectively,[52] together with the C-N-C peak at 285.9 eV, confirms the supporting of β-NA on the surface of GO-D.

Table 1 Analysis of the deconvoluted C1s peaks obtained from XPS and their relative atomic percentages for GO, GO-D and GO-N

Sample name	C1s fitting binding energy (eV) (relative atomic percentage %)								
	C=C	C-C	C-NH_2	C-OH	C-N-C	C-O-C	N-C=O	C=O	O-C=O
GO	284.5 (29.4)	284.9 (8.55)		285.8 (9.40)		286.8 (42.7)		288.2 (5.39)	289.1 (4.53)
GO-D	284.3 (28.5)	284.4 (42.0)		285.8 (8.94)	286.1 (4.68)	286.8 (9.29)		288.0 (3.52)	289.2 (2.97)
GO-N	284.1 (27.5)	284.9 (43.6)	285.4 (3.93)	285.7 (7.12)	285.9 (4.24)	286.5 (6.38)	287.4 (3.44)	288.2 (1.92)	289.3 (1.84)

Fig. 3 shows the XRD patterns of NG, GO, GO-D, GO-N and β-NA. The strong and sharp peak at 2θ of 26.5° in the XRD pattern of NG originates from the interlayer (002) spacing (d= 0.34 nm). After oxidation and exfoliation under ultrasonication, this sharp peak completely disappeared and a new broad peak appeared at 2θ = 8.8°, indicating that the neighboring layers are 1.0 nm apart because of the presence of oxygen groups on the surface of GO. Compared with the diffraction of GO, the diffraction peak of GO-D shifts to 4.2° from 8.8°, corresponding to the increase of intra-gallery spacing from 1.0 nm to 2.1 nm. The enlarged inter-layer space also indicates that ODA

has been intercalated into the layers of GO. In addition, the broad diffusion peak with the peak maxima at approximately at 20.6 ° (d = 0.42 nm) and a drastic reduction in peak intensity is observed for GO-D. This fact may be attributed to the formation of certain degree of reaggregated GO-D sheets during the refluxing process.[53] After further supporting of β-NA, the new diffraction peaks located at 2θ = 18.1° and 21.6° appear in the XRD trace of GO-N. Because all of these peaks correspond to the crystalline structure of β-NA, their presence demonstrates that the β-NA supported on GO-D can form crystals, which will then induce the formation of β crystals of iPP by epitaxial crystallization.[54] Moreover, compared with those of pristine β-NA, the positions of the diffraction peaks of GO-N shift slightly, which may be due to the interaction between β-NA and GO-D. The interlayer spacing of graphene is d=1.7 nm (2θ = 5.2°), implying the ease of complete exfoliation of graphene oxide in xylene solution and the iPP matrix.

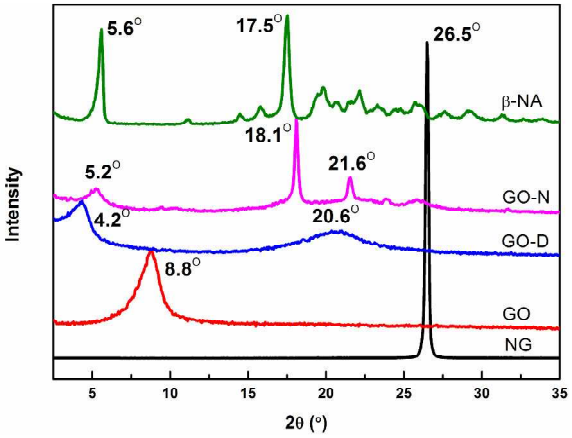

Fig. 3 XRD patterns of NG, GO, GO-D, GO-N and β-NA.

Crystallization behavior and crystalline structure of iPP nanocomposites

Fig.4 shows the DSC cooling and melting curves of pure iPP and iPP composites. From Fig.4a, the crystallization temperature (T_c) of iPP composites with 0.1 wt% GO-D is slightly higher than that of pure iPP, while that of iPP composites with 0.1 wt% GO is lower than pure iPP, indicating the

different effect of GO and GO-D on the crystallization of iPP. The slight hindering effect of GO and enhanced heterogeneous nucleating ability of GO-D on the crystallization of iPP can be confirmed by isotherm crystallization behavior (Fig.S1-3 and Table S1). The presence of GO-N improves T_c of iPP dramatically, and T_c increases with the content of GO-N increasing. These results strongly confirm the nucleating ability of the GO-N in iPP matrix. From Fig.4b, for pure iPP, and iPP composites with 0.1 wt% GO and GO-D, a single endothermic peak above 160 °C appears on the melting curves, showing that complete α crystals with no β crystals are formed. For iPP composites with GO-N, two endothermic peaks are observed at ca.150 and 168 °C, indicating the melting of β phase and α phase, respectively.

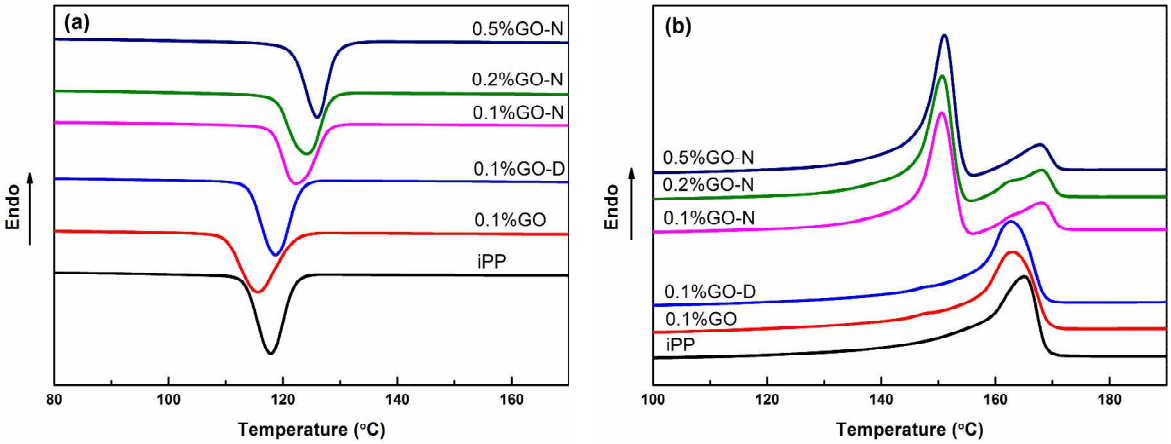

Fig.4 DSC (a) cooling and (b) melting curves of pure iPP and iPP composites.

XRD patterns of pure iPP and iPP composites are shown in Fig.5. No conspicuous diffraction peaks are observed except the crystalline diffraction peaks of the iPP matrix, indicating that no significant stacking of graphene oxide sheets occurs when dispersed in the iPP matrix. Consistent with DSC results, diffraction peaks of α(110), α(040) and α(130), corresponding to 2θ of 14.1°, 16.8°, and 18.6° respectively, are seen in pure iPP, and iPP composites with 0.1 wt % GO and GO-D. An additional strong diffraction peak of β(300) at 2θ of 16° appears on the XRD patterns of iPP

composites with GO-N, indicating the formation of β phase as well. The relative contents of β crystals (k_β) in the crystalline phase are 73.6%, 90.4% and 90.1% for iPP composites with GO-N content of 0.1, 0.2 and 0.5 wt%, respectively. Both the DSC and XRD results indicate that GO-N is an effective compound β nucleating agent for iPP at a low concentration, and the functionalized GO with β-NA can induce the formation of β crystals effectively. It should be noted that the nucleating ability of GO-D supported β-NA for β phase of iPP in this work is much higher than that of carbon nanotubes (CNTs) supported β-NA in our previous work[43], in the latter the maximum k_β is only 12.48% at the content of 1% CNTs supported β-NA. The nucleation theory suggests that curved surfaces of CNTs make it harder for nucleation to occur.[55, 56] More importantly, two-dimensional carbons of GO-D are more favorable to the deposition of β-NA onto the surface of graphene platelets.

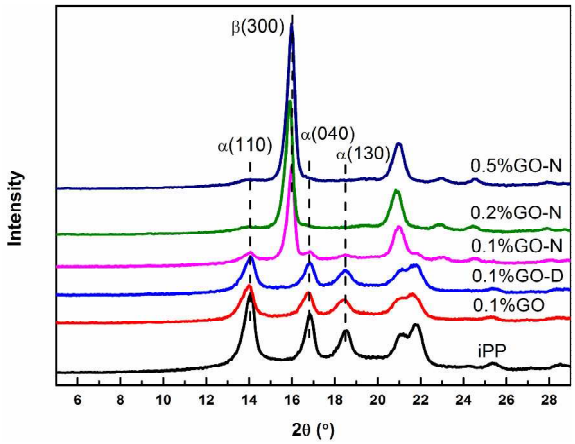

Fig.5 XRD patterns of pure iPP and iPP composites.

Mechanical properties of iPP composites

Fig.6 shows the impact strength, tensile strength, and elongation at break of pure iPP and iPP composites. As shown in Fig. 6(a), GO-D filled iPP sample shows higher tensile strength with no sacrifice of toughness. However, the impact strength of GO modified iPP is inferior to that of pure

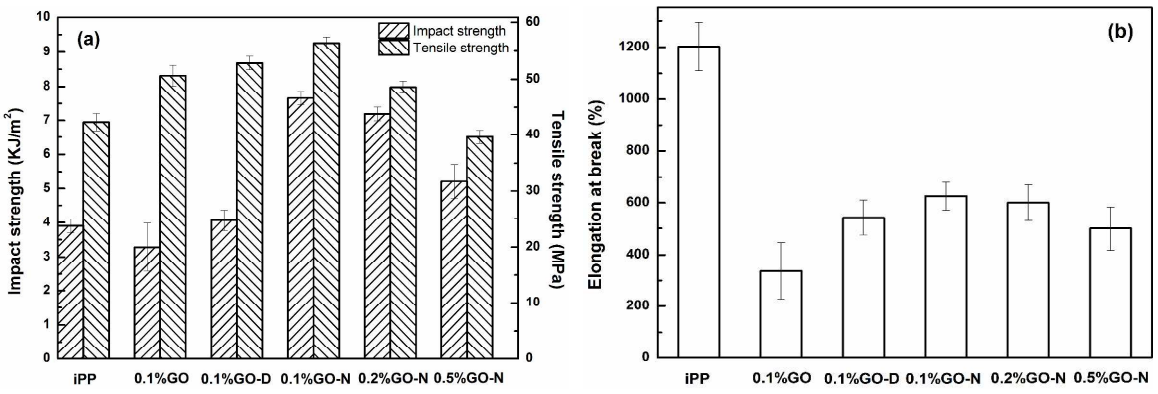

Fig.6 (a) Impact strength and tensile strength and (b) elongation at break of pure iPP and iPP composites.

iPP, and the reinforcing effect is less obvious than that of GO-D. The impact strength of iPP composites with GO-N are largely improved compared with that of pure iPP and iPP composites with GO and GO-D. A maximum improvement of nearly 100% in impact strength compared with that of pure iPP is achieved at 0.1 wt% GO-N loading, and with the content of GO-N increasing, the increase of impact strength weakens. Interestingly, the tensile strength also increases over pure iPP when the content of GO-N is lower than 0.5 wt%, and the tensile strength of iPP composites with 0.1% GO-N is even higher than that of composites with 0.1% GO-D. As shown in Fig. 6(b), compared with GO-D, GO has more negative effect on the elongation at break. Although the elongation at break decreases for all the iPP composites with GO-N compared with pure iPP, it still maintains at a very high level. With the content of GO-N increasing, the elongation at break decreases, but it still higher than that of iPP composites with 0.1% GO-D when the loading of GO-N lower than 0.5 wt%. The impact strength, tensile strength and elongation at break achieve the maximum improvement at the same loading of 0.1 wt% GO-N. The results show that iPP is toughened and reinforced simultaneously by GO-N and this reinforcement in mechanical properties is highly influenced by the dispersion state of the filler and the interface between the filler and matrix,

which will be discussed in the following section. However, further increasing the content of GO-N from 0.2 to 0.5 wt% leads to the decrease of the impact strength, tensile strength and elongation at break, which may be due to the aggregation of graphene oxide sheets by the Vander Waals force.

Structure-property relationship

ODA is mainly used as a surface modifier to improve the hydrophobicity of GO and its dispersion in non-polar polymers. Fig.7 shows the dispersion of GO, GO-D and GO-N in the immiscible xylene/water mixture (1mg/ml, v_{xylene} / v_{water} =1/1). The unfunctionalized and functionalized GO exhibit totally different affinities. Compared to GO, which tends to be dispersed in polar water (lower layer), GO-D and GO-N are lifted to nonpolar xylene (upper layer), an important nonpolar solvent which can dissolve most important nonpolar polymers, including iPP. The conversion of the hydrophilic feature of GO to the hydrophobic characteristics of GO-D confirms the effectiveness of surface functionalization. The results clearly indicate that the substitute alkyl groups in GO-D change the surface nature of GO, and further supporting of β-NA does not change its solubility in xylene.

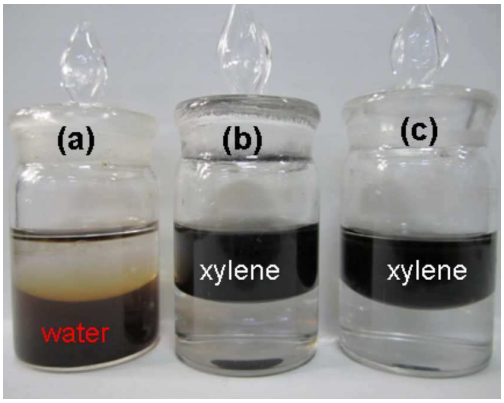

Fig.7 Dispersion of (a) GO, (b) GO-D and (c) GO-N in the immiscible xylene/water mixture (1mg/ml, v_{xylene} / v_{water} =1/1).

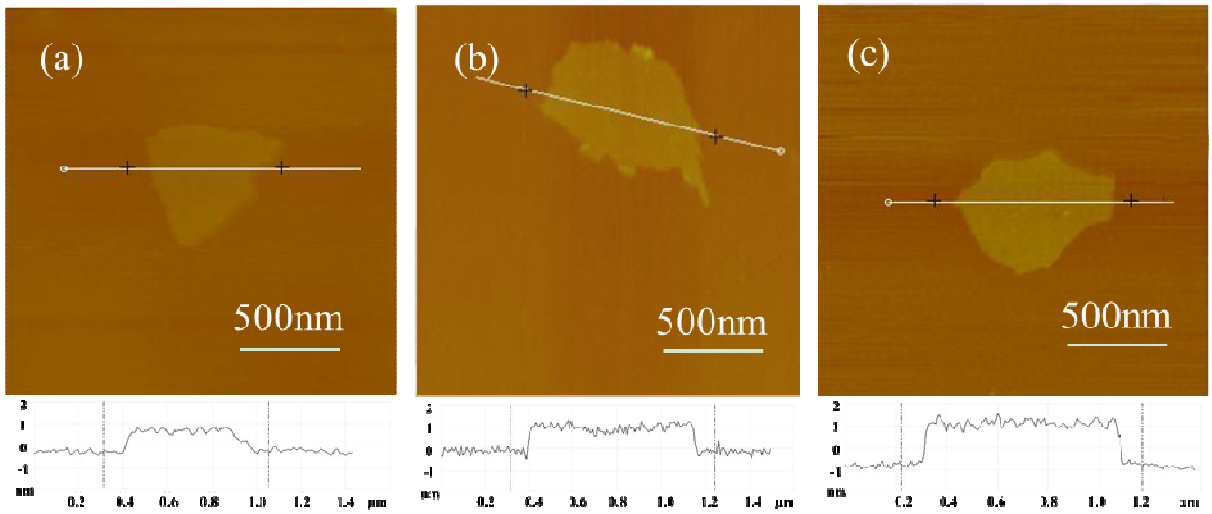

Fig. 8 AFM images and line profiles of (a) GO deposited from a dispersion in water, (b) GO-D and (c) GO-N deposited from a dispersion in xylene.

To give the degree of exfoliation of GO, GO-D and GO-N in the solvents, AFM imaging of the dispersions deposited on mica substrates was carried out. Fig. 8 shows the AFM images and line profiles of GO deposited from a dispersion in water and GO-D and GO-N deposited from a dispersion in xylene. The thicknesses of GO sheets determined from AFM images are about 0.90 nm, which agrees with the previous reports of monolayer of GO.[57] Due to the grafting of long alkyl chains, the thicknesses of GO-D are seen to rise to about 1.37 nm, which also agrees with the reports of ODA functionalized GO[35]. The thicknesses of GO-N further increase to about 1.93 nm, which should be attributed to the subsequent supporting of β-NA. To further perceive the exfoliation state and morphology of GO-N sheets in the iPP composites, a microtomed crosssection of iPP composites with 0.1 wt% GO-N was analyzed by TEM. As is shown in Fig. 9, multilayered GO-N sheets exhibiting a wrinkled structure were seen, suggesting that the GO-N particles are not completely exfoliated into individual sheets. However, according to the XRD results, there is a high possibility that many few-layered or monolayered platelets, which may be "invisible" by TEM[58], were dispersed

in the iPP matrix.

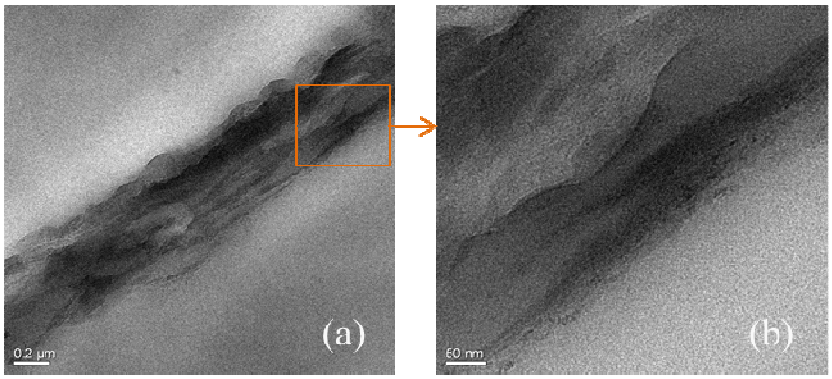

Fig. 9 TEM images of (a) microtomed cross-sections of iPP composites with 0.1 wt% GO-N and (b) the partial enlarged view.

Fig. 10 shows SEM micrographs for the supermolecular structures of etched pure iPP and iPP composites. Typical α-spherulites can be observed for pure iPP, iPP composites with 0.1 wt % GO and GO-D, and the boundaries between α-spherulites are clear (Fig. 10a-c). For pure iPP, the diameters of α-spherulites are heterogeneous. The diameters of α-spherulites are reduced and the size uniformity is enhanced for iPP composites with GO-D, due to enhanced heterogeneous nucleating ability of GO-D on the crystallization of iPP as shown in Fig.4a, Fig.S1-3 and Table S1. From Fig. 10d-f, the typical bundlelike morphology of β-spherulites with no clear boundaries appears in iPP composites with GO-N. With the content of GO-N increasing from 0.1 wt% to 0.2 wt%, the sizes of β-spherulites decrease dramatically, also indicating the nucleating role of the GO-N in the iPP matrix. It should be noted that, for iPP composites with GO-N, a few α crystals and a large number of β crystals can be detected by DSC and WAXD measurements. However, SEM micrographs show that the whole area of the etched sample is filled with crystalline superstructures that can be assigned to β phase due to the high β phase content.

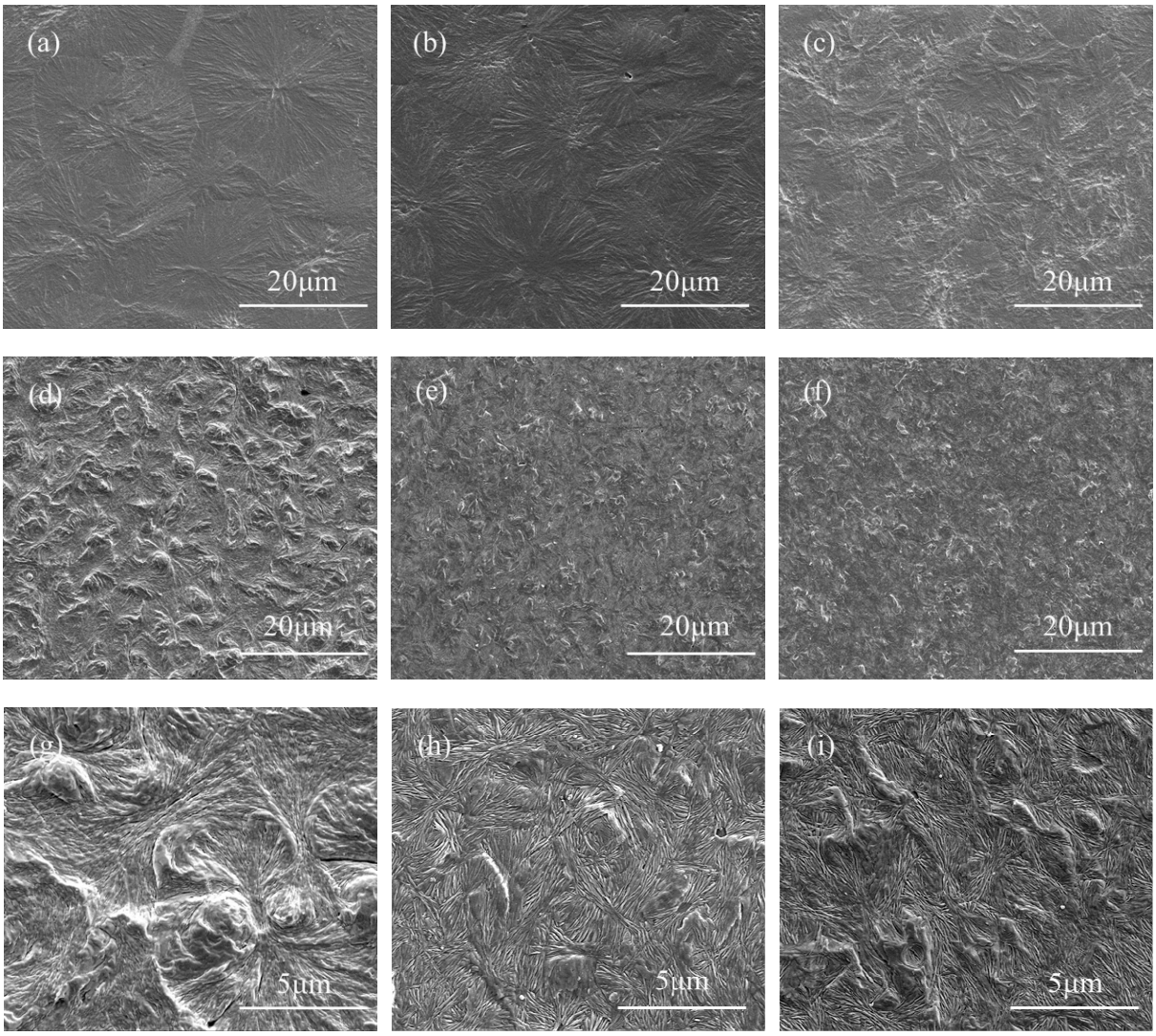

Fig. 10 SEM micrographs for the supermolecular structures of etched pure iPP (a) and iPP composites with 0.1 wt% GO (b), 0.1 wt% GO-D (c), 0.1 wt% GO-N (d), 0.2 wt% GO-N (e), and 0.5 wt% GO-N (f). (g), (h) and (i) are magnified micrographs of (c), (d), and (e), respectively.

To illustrate the structure-property relationship, the schematic representation of crystalline structure and morphology of iPP composites with GO, GO-D, and GO-N is shown in Fig. 11. As shown in Fig. 11a, α crystals can be induced by GO and GO-D, and interface between filler and matrix is bridged by α crystalline layer mainly. A large number of β crystals can be induced by GO-N,

and SEM micrographs show β-spherulites can be formed in iPP composites with GO-N (Fig.10d-i). The lamellae of β phase can grow on the both surfaces of GO-N due to its nucleation ability to β crystals, and then GO-N is embedded in β-spherulites. The core-shell like structure with GO as the core and lamella of β crystals as the shell is obtained in α-iPP matrix in Fig. 11b. The strong polymer/filler interaction can be achieved by the presence of the β crystal layer.

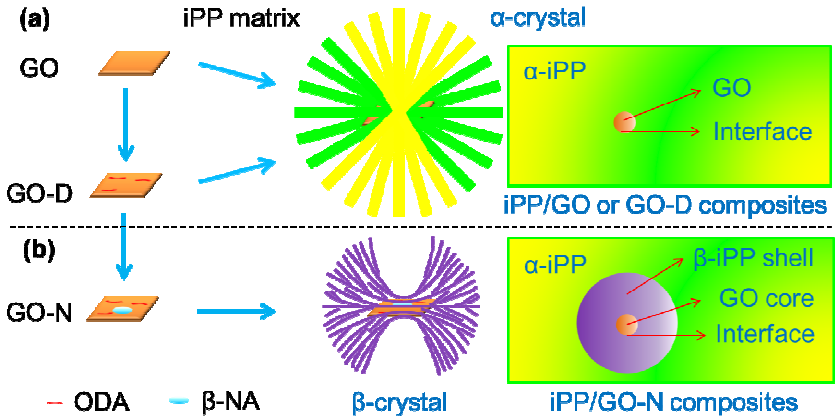

Fig. 11. Schematic representation of crystalline structure and morphology of iPP composites with GO, GO-D, and GO-N.

Fig.12 gives the bright field TOM photographs showing the crack initiation patterns of pure iPP and iPP composites from the damage zone of the unbroken notch of the DN-4-PB tests. For pure iPP and iPP composites with 0.1 wt % GO and GO-D as shown in Fig.12a-c, a few crazing spreads into the matrix at the crack tip, which is well consistent with the low notch impact strength. Compared to pure iPP, the magnitude of crazing is higher for iPP composites with GO-D, while it is lower for iPP composites with GO. The ratios of the crazed area for iPP composites with 0.1 wt% GO and 0.1 wt% GO-D to that of iPP are 0.72, and 1.55, respectively. Indeed, the size of the damage (craze) zone scales with the impact strength results. From Fig.12d-f, there is distinctively different fracture mechanism in the iPP samples with GO-N. Yield-region takes place around the crack tip and it

should be noted that no sign of crack propagation is observed in iPP composites with GO-N, implying better ability of preventing crack propagation. With the content of GO-N increasing, smaller yield-region can be seen, which is consistent with the decreased notch impact strength. The ratios of the yield-region area for iPP composites with 0.1 wt%, 0.2 wt%, and 0.5 wt% GO-N to that of iPP are 7.00, 6.35 and 5.34, respectively.

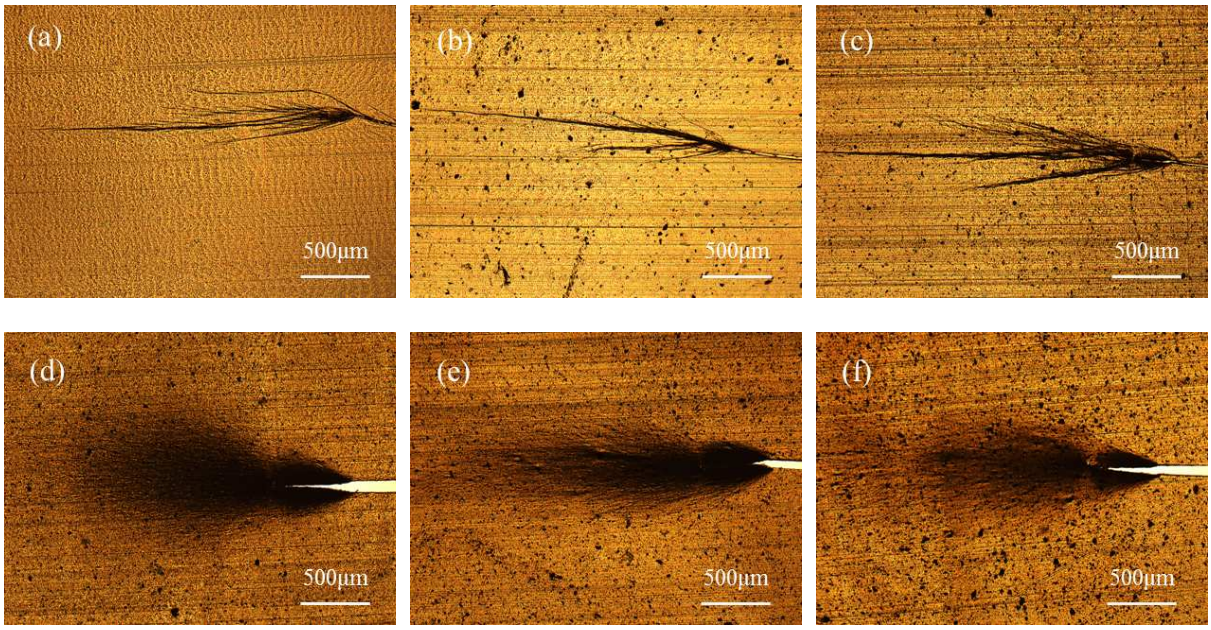

Fig.12 Bright field TOM photographs showing the crack initiation patterns of pure iPP (a) and iPP composites with 0.1 wt% GO (b), 0.1 wt% GO-D (c), 0.1 wt% GO-N (d), 0.2 wt% GO-N (e), and 0.5 wt% GO-N (f) from the damage zone of the unbroken notch of the DN-4-PB tests.

The above mentioned interface between nanofillers and polymer matrix, crystalline structure and morphology of polymer matrix are key factors that affect the performance of polymer composites. The addition of GO can enhance the tensile strength of iPP, but there is a decrease in toughness due to the poor compatibility between iPP and GO. ODA improve the hydrophobicity of GO and its dispersion in iPP, then the tensile strength for iPP composites with GO-D is increased

further. For iPP composites with GO-D, α crystals are also the exclusively crystalline structure. So, the slight improvement of toughness described above is mainly ascribed to the sharp decrease of the diameter of spherulites and their homogeneous dispersion due to enhanced heterogeneous nucleating ability of GO-D on the crystallization of iPP.

The further supporting of β-NA does not change the surface nature of GO-D, and improved homogeneous dispersion in xylene and interfacial adhesion with non-polar iPP matrix can be observed in Fig. 7. The functionalized GO with β-NA induce the formation of β crystals effectively as shown by DSC and XRD results in Fig. 4 and 5. The significant improvement in toughness can be ascribed to the formation of a large number of β crystals of iPP. As shown in Fig. 10 and 11, different morphology of α crystals and β crystals appear in iPP composites. α phase of iPP shows excellent modulus, tensile strength but inferior fracture toughness because of the radial lamellae by the tangential crystallite which makes the plastic deformation very difficult [59, 60]. However, β crystals of iPP without cross-hatching allow the initiation and propagation of plastic deformation more easily and then enhance the energy dissipating process [61, 62]. Karger-Kocsis attributes the enhanced toughness of β phase of iPP to a stress-induced transformation from less denser β form to denser α form crystalline structure at the root of a growing crack[63]. As shown in Fig.12, the yield-region takes place around the crack tip for iPP composites with GO-N due to the formation of β crystals with bundlelike morphology, while crazing spreads into the matrix at the crack tip for pure iPP and iPP composites with GO and GO-D in which only α-spherulites can be observed. Thus, the large number of β crystals formed in the composites is the major reason for the improved fracture toughness of iPP.

The creation of a polymer crystalline layer bridging the nanofillers and the polymer matrix is

considered a promising way to engineer a strong non-covalent interface for stress transfer in polymer composites.[39, 40] As confirmed by DSC and XRD results, GO-N shows effective β nucleating ability for iPP. Stronger interfacial interaction between polymer matrix and filler can be achieved by interfacial crystallization induced by the supporting of β-NA. On the other hand, the core-shell like structure with GO as core and lamella of β crystals as shell is obtained in α-iPP matrix as shown in Fig. 11b. This structure is difficult to observe directly due to the bulk crystallization in composites, and will be evidenced in our further work. The core-shell structure is very effective in balancing the stiffness-toughness of the material. [64, 65] It is then interesting to note that the tensile strength of iPP composites with 0.1 wt% GO-N is even higher than that of iPP composites with 0.1 wt% GO-D, though high content of β crystals with lower stiffness are formed. As the content of GO-N increasing, k_β increases to 90%. The decrease of α crystals and poorer GO-N dispersion owing to higher GO-N loading lead to the less effect on toughness and tensile strength. As shown in Fig.S4, at the loading of 0.5 wt%, the aggregation of GO-N can easily observed on the impact fractured surface of iPP composites, causing nonuniform dispersion of reinforcement phase, which leads to localized stress concentration. Then smaller yield-region can be seen for iPP composites with the content of GO-N increasing as shown in Fig.12.

Moreover, the good interfacial adhesion between GO-D and iPP weaken the negative effect of GO on the elongation at break of iPP, and the formation of β crystals layer on the surface can further reduce this effect due to the effective stress transfer across the noncovalent interface. Although the aggregation of GO-N increases with the content of GO-N increasing, the elongation at break of iPP composites with 0.5 wt% GO-N is still higher than that of with 0.1 wt% GO.

Conclusion

The surface functionalization of GO was realized by grafting of ODA, and then supporting of β-NA for iPP. iPP samples modified by this compound β-NA show simultaneously enhanced toughness and tensile strength. Due to the alkylation of GO, the compound β-NA can disperse in non-polar solvent. The improved interfacial adhesion and compatibility lead to enhanced heterogeneous nucleating ability and its nucleating ability for β phase of iPP is granted by the supported β-NA. With only 0.1 wt% loading of the compound β- NA, the k_β value can reach 73.6%; The impact strength of iPP composites reach a maximum increase by almost 100%, and the tensile strength achieved an increase of about 30%, showing excellent toughening and reinforcing effect by this interfacial crystalline structure control. The results are very significant in obtaining a material having remarkable stiffness-toughness balance.

Acknowledgment

This work was supported by the National Natural Science Foundation of China (NNSFC Grants 21374065, 51121001), the MOST (Grant No. 2011CB606006, 2012CB025902) and the Fundamental Research Funds for the Central Universities (Grant No. 2011SCU04A03). The authors also thank Mr. Chao-liang Zhang for his kind assistance in morphological observations.

References

1 F. Luo, C. Geng, K. Wang, H. Deng, F. Chen, Q. Fu and B. Na, *Macromolecules*, 2009, **42**, 9325.

2 J. Varga, *J. Macromol. Sci. Phys*, 2002, **41**, 1121.

3 S. W. Wang, W. Yang, R. Y. Bao, B. Wang, B. H. Xie and M. B. Yang, *Colloid Polym. Sci.*, 2010, **288**, 681.

4 J. Varga and A. Menyhárd, *Macromolecules*, 2007, **40**, 2422.
5 A. T. Jones, J. M. Aizlewood and D. Beckett, *Macromol. Chem. Phys.*, 1964, **75**, 134.
6 Y. Fujiwara, *Colloid Polym. Sci.*, 1975, **253**, 273.
7 D. Byelov, P. Panine, K. Remerie, E. Biemond, G. C. Alfonso and W. H. de Jeu, *Polymer*, 2008, **49**, 3076.
8 Z. Zhang, C. Wang, Z. Yang, C. Chen and K. Mai, *Polymer*, 2008, **49**, 5137.
9 J. Varga and A. Menyhard, *Macromolecules*, 2007, **40**, 2422.
10 H. Bai, Y. Wang, Z. Zhang, L. Han, Y. Li, L. Liu, Z. Zhou and Y. Men, *Macromolecules*, 2009, **42**, 6647.
11 C. Lee, X. Wei, J. W. Kysar and J. Hone, *Science*, 2008, **321**, 385.
12 K. Novoselov, A. K. Geim, S. Morozov, D. Jiang, M. K. I. Grigorieva, S. Dubonos and A. Firsov, *Nature*, 2005, **438**, 197.
13 A. A. Balandin, S. Ghosh, W. Bao, I. Calizo, D. Teweldebrhan, F. Miao and C. N. Lau, *Nano Lett.*, 2008, **8**, 902.
14 A. A. Balandin, *Nature Mater.*, 2011, **10**, 569.
15 A. K. Geim and K. S. Novoselov, *Nature Mater.*, 2007, **6**, 183.
16 M. Liang and L. Zhi, *J. Mater. Chem.*, 2009, **19**, 5871.
17 F.-Y. Su, C. You, Y.-B. He, W. Lv, W. Cui, F. Jin, B. Li, Q.-H. Yang and F. Kang, *J. Mater. Chem.*, 2010, **20**, 9644.
18 S.-Y. Yang, K.-H. Chang, H.-W. Tien, Y.-F. Lee, S.-M. Li, Y.-S. Wang, J.-Y. Wang, C.-C. M. Ma and C.-C. Hu, *J. Mater. Chem.*, 2010, **21**, 2374.
19 G. P. Keeley, A. O'Neill, N. McEvoy, N. Peltekis, J. N. Coleman and G. S. Duesberg, *J. Mater. Chem.*, 2010, **20**, 7864.
20 J. T. Robinson, F. K. Perkins, E. S. Snow, Z. Wei and P. E. Sheehan, *Nano Lett.*, 2008, **8**, 3137.
21 R. I. Jafri, N. Rajalakshmi and S. Ramaprabhu, *J. Mater. Chem.*, 2010, **20**, 7114.
22 J. Cheng, G. Zhang, J. Du, L. Tang, J. Xu and J. Li, *J. Mater. Chem.*, 2011, **21**, 3485.
23 V. Goyal and A. A. Balandin, *Appl. Phys. Lett.*, 2012, **100**, 073113.
24 X. Yang, X. Zhang, Y. Ma, Y. Huang, Y. Wang and Y. Chen, *J. Mater. Chem.*, 2009, **19**, 2710.
25 D. Cai and M. Song, *J. Mater. Chem.*, 2010, **20**, 7906.
26 R. Verdejo, M. M. Bernal, L. J. Romasanta and M. A. Lopez-Manchado, *J. Mater. Chem.*, 2011, **21**, 3301.
27 Z. Xu and C. Gao, *Macromolecules*, 2010, **43**, 6716.
28 O. K. Park, J. Y. Hwang, M. Goh, J. H. Lee, B. C. Ku and N. H. You, *Macromolecules*, 2013, **46**, 3505.
29 G.-Q. Qi, J. Cao, R.-Y. Bao, Z.-Y. Liu, W. Yang, B.-H. Xie and M.-B. Yang, *J. Mater. Chem. A*, 2013, **1**, 3163.
30 Y. Zhu, S. Murali, W. Cai, X. Li, J. W. Suk, J. R. Potts and R. S. Ruoff, *Adv. Mater.*, 2010, **22**, 3906.
31 Y. Cao, J. Feng and P. Wu, *J. Mater. Chem.*, 2012, **22**, 14997.
32 D. R. Dreyer, S. Park, C. W. Bielawski and R. S. Ruoff, *Chem. Soc. Rev.*, 2010, **39**, 228.
33 J. R. Potts, S. H. Lee, T. M. Alam, J. An, M. D. Stoller, R. D. Piner and R. S. Ruoff, *Carbon*,

2011, **49**, 2615.
34 J. J. Liang, Y. Huang, L. Zhang, Y. Wang, Y. F. Ma, T. Y. Guo and Y. S. Chen, *Adv. Funct. Mater.*, 2009, **19**, 2297.
35 Y. Cao, J. Feng and P. Wu, *Carbon*, 2010, **48**, 1683.
36 T. Kuila, S. Bose, A. K. Mishra, P. Khanra, N. H. Kim and J. H. Lee, *Prog. Mater. Sci.*, 2012, **57**, 1061.
37 W. Li, X. Z. Tang, H. B. Zhang, Z. G. Jiang, Z. Z. Yu, X. S. Du and Y. W. Mai, *Carbon*, 2011, **49**, 4724.
38 Y. S. Yun, Y. H. Bae, D. H. Kim, J. Y. Lee, I. J. Chin and H. J. Jin, *Carbon*, 2011, **49**, 3553.
39 J. N. Coleman, M. Cadek, R. Blake, V. Nicolosi, K. P. Ryan, C. Belton, A. Fonseca, J. B. Nagy, Y. K. Gun'ko and W. J. Blau, *Adv. Funct. Mater.*, 2004, **14**, 791.
40 D. Y. Cai and M. Song, *Nanotechnology*, 2009, **20**.
41 H. Wang, P.-G. Ren, Y.-H. Chen, D.-X. Yan, Z.-M. Li and L. Xu, *J. Appl. Polym. Sci.*, 2013, DOI: 10.1002/app.40000.
42 J. Z. Xu, Y. Y. Liang, H. D. Huang, G. J. Zhong, J. Lei, C. Chen and Z. M. Li, *J. Polym. Res.*, 2012, **19**.
43 K. J. Zhan, W. Yang, L. Yue, B. H. Xie and M. B. Yang, *J. Macromol. Sci. Phys.*, 2012, **51**, 2412.
44 W. S. Hummers and R. E. Offeman, *J. Am. Chem. Soc.*, 1958, **80**, 1339.
45 J. Cao, Y. Wang, K. Ke, Y. Luo, W. Yang, B. H. Xie and M. B. Yang, *Polym. Int.*, 2012, **61**, 1031.
46 G.-Q. Qi, J. Cao, R.-Y. Bao, Z.-Y. Liu, W. Yang, B.-H. Xie and M.-B. Yang, *J. Mater. Chem. A*, 2013, **1**, 3163.
47 G. Wang, X. Shen, B. Wang, J. Yao and J. Park, *Carbon*, 2009, **47**, 1359.
48 Z. Lin, Y. Liu and C. Wong, *Langmuir*, 2010, **26**, 16110.
49 R. H. Olley and D. C. Bassett, *Polymer*, 1982, **23**, 1707.
50 D. Chen, H. Feng and J. Li, *Chem. Rev.*, 2012, **112**, 6027.
51 R. Larciprete, S. Fabris, T. Sun, P. Lacovig, A. Baraldi and S. Lizzit, *J. Am. Chem. Soc.*, 2011, **133**, 17315.
52 M.-C. Hsiao, S.-H. Liao, Y.-F. Lin, C.-A. Wang, N.-W. Pu, H.-M. Tsai and C.-C. M. Ma, *Nanoscale*, 2011, **3**, 1516.
53 A. M. Shanmugharaj, J. H. Yoon, W. J. Yang and S. H. Ryu, *J. Colloid Interface Sci.*, 2013, **401**, 148.
54 W. Stocker, M. Schumacher, S. Graff, A. Thierry, J.-C. Wittmann and B. Lotz, *Macromolecules*, 1998, **31**, 807.
55 N. H. Fletcher, *J. Chem. Phys.*, 1958, **29**, 572.
56 A. Cacciuto, S. Auer and D. Frenkel, *Nature*, 2004, **428**, 404.
57 S. Stankovich, D. A. Dikin, R. D. Piner, K. A. Kohlhaas, A. Kleinhammes, Y. Jia, Y. Wu, S. T. Nguyen and R. S. Ruoff, *Carbon*, 2007, **45**, 1558.
58 J. R. Potts, S. Murali, Y. Zhu, X. Zhao and R. S. Ruoff, *Macromolecules*, 2011, **44**, 6488.
59 G. Coulon, G. Castelein and C. G'sell, *Polymer*, 1999, **40**, 95.
60 M. Aboulfaraj, C. G'sell, B. Ulrich and A. Dahoun, *Polymer*, 1995, **36**, 731.

61 H. Chen, J. Karger-Kocsis, J. Wu and J. Varga, *Polymer*, 2002, **43**, 6505.
62 J. Karger-Kocsis, J. Varga and G. Ehrenstein, *J. Appl. Polym. Sci.*, 1997, **64**, 2057.
63 J. Karger-Kocsis, *Polym. Eng. Sci.*, 1996, **36**, 203.
64 K. Wang, Y. Chen and Y. Zhang, *Polymer*, 2009, **50**, 1483.
65 D. Kaempfer, R. Thomann and R. Mülhaupt, *Polymer*, 2002, **43**, 2909.